

## Temperature and leaching effects of zeolite-X derived from kaolin

Henry E. Mgbemere<sup>\*1</sup>, Henry Ovri<sup>2</sup> and Anna-Lisa Sargent<sup>3</sup>

<sup>1</sup>Department of Metallurgical and Materials Engineering, University of Lagos, Akoka, Lagos State, Nigeria

<sup>2</sup>Experimental Materials Mechanics, Institute of Materials Research, Helmholtz Zentrum Hereon.  
Max Planck Strasse 1, 21502 Geesthacht Germany

<sup>3</sup>Department of Nanotechnology, Institute of Materials Research, Helmholtz Zentrum Hereon.  
Max Planck Strasse 1, 21502 Geesthacht Germany

(Received November 24, 2021, Revised December 16, 2021, Accepted July 17, 2023)

**Abstract.** Zeolites are microporous materials that find applications in different fields due to their numerous interesting properties. This research investigated the effect of leaching on unheated Ifon kaolin in dilute hydrochloric acid and sulphuric acid. The hydrothermal method synthesized zeolite-X type, and the resulting sample was characterized using different techniques. The silica/alumina ratio in the synthesized sample was approximately 5.6, while Infrared spectra confirmed that the synthesized material was Zeolite-X. Based on the X-ray diffraction patterns, other phases were also formed in addition to zeolite-X crystals. Thermogravimetry results indicated that the synthesized zeolite was relatively stable below 500°C, so its weight loss was only 13% after heating to about 200°C. A differential thermal analyzer confirmed this amount of weight loss, and endothermic and exothermic reactions were also observed for the samples calcined respectively at 700 and 900°C. Based on Brunauer-Emmett-Teller (BET) analyses, samples at 700°C showed slower adsorption-desorption isotherms, pore volume, and sizes than those at 900°C. These results have shown that leaching and calcination temperature significantly affect the type of zeolite produced.

**Keywords:** hydrothermal synthesis; Ifon kaolin; metakaolin; processing; zeolite X

### 1. Introduction

Zeolites are microporous, crystalline materials with three main components: framework tetrahedral, adsorbed molecules, and cations (Khaleque *et al.* 2020, Verboekend *et al.* 2016). These characteristics enable them to have various applications depending on their particular framework structures (Li *et al.* 2013). However, some zeolites with the same framework structure can exhibit different properties (Król 2020, Li *et al.* 2013). They are generally used as catalysts in oil refining, as molecular sieves for filtration, and as water softeners for water purification. Zeolites exist in nature and can also be synthesized in the laboratory, and those found in nature usually contain impurities. Synthetic chemicals are the main source of raw materials or precursors used in producing most zeolites today. This is because, for most applications, a high degree of purity is required

---

\*Corresponding author, Ph.D., E-mail: hmgbemere@unilag.edu.ng

(Abdullahi *et al.* 2017). Some chemicals used include sodium aluminate, aqueous tetramethyl ammonium hydroxide, aluminium isopropoxide, silica gel, etc. (Khaleque *et al.* 2020).

The challenge with using synthetic materials or precursors to produce zeolites is that the production cost is higher than natural raw materials (Andrade *et al.* 2020, Mgbemere *et al.* 2018). In most developing countries, alumina and silica-rich raw materials with compositions suitable for zeolite processing are abundant. Some of these raw materials include coal gangue (Chen and Lu 2018), coal fly ash (Ojumu *et al.* 2016, Zhu *et al.* 2019), sand mine (Andrade *et al.* 2020), kaolin (Alaba *et al.* 2017, Khalifah *et al.* 2018), etc. Kaolin is one of the most abundant sources of alumina and silica and also contains a substantial quantity of impurities that tend to limit its application. Another challenge is that its composition varies from location to location. It has, however, been used to produce different types of zeolites like zeolite A (Chen and Lu 2018, Kirdeciler and Akata, 2020), ZSM5 zeolite (Hartanto *et al.* 2017), zeolite-X (Ifitahiyah *et al.* 2018, Otieno *et al.* 2021), and zeolite-Y (Adeoye *et al.* 2017, Khalifah *et al.* 2018, Pavlov *et al.* 2015). Different techniques have been used to reduce the number of impurities and produce acceptable zeolites. Kaolin containing significant amounts of both  $\text{Fe}_2\text{O}_3$  and  $\text{TiO}_2$  has been leached with HCl,  $\text{H}_2\text{SO}_4$ , and  $\text{CH}_3\text{COOH}$ , leading to a considerable reduction (>50%) in these impurities (Chouafa *et al.* 2015). Kaolin from Kankara in Nigeria has been leached with  $\text{H}_2\text{SO}_4$  and processed to form zeolites having mixed characteristics and types (Atta *et al.* 2007). Other methods that have been used for zeolite synthesis include hierarchical zeolites using acid-activated kaolin (Alaba *et al.* 2015), a three-step hydrothermal reaction of the precursors (Ifitahiyah *et al.* 2018), the addition of surfactant in kaolin to create a template (Khalifah *et al.* 2018), thermal activation in one pot by alkali fusion (Kirdeciler and Akata 2020), kaolin pretreatment and changes in NaOH levels before fusion (Otieno *et al.* 2021), the addition of polyvinyl alcohol (Pavlov *et al.* 2015), a split technique involving the splitting of kaolin into  $\text{Al}_2\text{O}_3$  and  $\text{SiO}_2$  (Salahudeen and Ahmed 2017), and a two-step hydrothermal method for zeolite-X (Srilai *et al.* 2019). The reaction temperature and impurity levels are among the important factors that affect the degree of zeolite formation starting from kaolin sources. Leaching of the kaolin using different concentrations of HCl and  $\text{H}_2\text{SO}_4$  has been used in this work. Two calcination temperatures (700°C and 900°C) were also used to synthesize zeolite-X. The objective is to study how different concentrations of acid and calcination temperature affect the properties of the zeolite-X produced.

## 2. Experimental procedure

The Kaolin used in this research was obtained from Ifon (located in Ondo state, Nigeria, with GPS coordinates 6.9235°N, 5.7774°E).

### 2.1 Sample preparation

Wet beneficiation of the kaolin was initially carried out to remove physically trapped impurities that can easily be removed with water. After decanting the top water, it was soaked for 24 h in distilled water. The resulting slurry was sieved using a mesh sieve with an aperture size of 75  $\mu\text{m}$  and allowed to dry. The cake-like mass was broken into smaller particles and then milled using a ball milling machine containing alumina balls 10 mm in diameter. The ratio of the ceramic balls to the kaolin is 10:1, while the milling duration was 6 h at a speed of 60 rpm.

The sample leaching was done using 1M HCl and 0.5 M  $\text{H}_2\text{SO}_4$ . Both acids were diluted with

distilled water by 7% and 15%, respectively. The kaolin was leached with HCl at room temperature for 30 mins while the H<sub>2</sub>SO<sub>4</sub> was at 80°C at a pH of 3. The leached kaolin was washed with distilled water, filtered, dried in an oven at 120°C, and crushed. The kaolin was calcined in a furnace at a controlled heating rate of 5°C/min to 700°C and 900°C, respectively, and held for 2 h before cooling in air. After calcination, the kaolin was transformed from an unreactive state to a reactive state called metakaolin. Sodium hydroxide (NaOH), and sodium silicate (Na<sub>2</sub>SiO<sub>3</sub>), were also used for the synthesis. The metakaolin was mixed with NaOH, Na<sub>2</sub>SiO<sub>3</sub>, and distilled water in a ratio of 1:1.14:3.43:17.14. The mixture was mechanically stirred intermittently and then aged gradually. The heating of the mixture in an oven at 100°C for 6 h resulted in gradual crystallization and grain growth. The zeolite was washed thrice with distilled water to ensure that any remaining NaOH was washed off. The solution was put inside a centrifuge at 20 rpm for 20 min to separate the zeolite from the water. The separated water was decanted, and the resulting zeolite-X sample was placed in an oven at 110°C for 6 h (Srilai *et al.* 2019).

## 2.2 Sample preparation

The chemical composition of the raw kaolin, and the zeolite-X crystals, were determined using an X-ray Fluorescence (XRF) analyzer (AXIOS, PAN Analytical, Netherland). A binder was added to the zeolite powder and pressed to form pellets for easy measurement. The Infrared spectra of the samples were determined using Fourier Transform Infrared Spectroscopy (Shimadzu IR Affinity-1S, Japan). The samples were prepared by pressing the powder to form a 6 mm diameter pellet using KBr as a binder in the sample-binder ratio of 11:3. The pellet was degassed at a temperature of 120°C for 1 h before acquiring the spectra with an average of 128 scans and resolution of 1 cm<sup>-1</sup>. The measurement was obtained in transmission mode from 400 to 4000 cm<sup>-1</sup>.

The thermal properties of the sample were determined using a Differential Thermal Analyser (Differential Thermal Analysis/Thermogravimetric (DTA/TG, Netzsch STA 409 C, Germany). This was carried out in an argon atmosphere with a 50 ml/min flow rate from 20 to 800°C at a heating and cooling rate of 5°C/min, respectively. The X-ray diffraction patterns of the samples were measured using an X-ray Diffractometer (Bruker D8 Discover, Karlsruhe, Germany) with CuK $\alpha$  radiation ( $\lambda=1.54056$  Å) operating at 1000  $\mu$ A and 50 kV. The samples were ground and placed in a sample holder in preparation for the measurement. The scanning range of the sample is from 10° to 80° at a scanning rate of 8.75° and an exposure time of 400 s per step.

The samples' specific surface area and gas adsorption data were determined using a Brunauer-Emmett-Teller (BET) adsorption analyzer (Micromeritics ASAP 2020 porosity analyzer, USA). The sample was first degassed at 80°C under vacuum for 40 h while the warm and cold free space values were determined using helium. Degassing was obtained in a vacuum at 350°C for 8 h, and N<sub>2</sub> sorption was used to determine the free space values.

## 3. Results and discussion

### 3.1 Chemical analysis

The chemical composition of Ifon kaolin (natural and leached) and those of the synthesized zeolite-X samples are shown in Table 1. The major compounds found in the kaolin are Al<sub>2</sub>O<sub>3</sub> and SiO<sub>2</sub> in quantities of approx. 38.2 and 41.53 wt.%, respectively. Other compounds present as minor

Table 1 Chemical composition analysis of Ifon kaolin and the synthesized zeolite-X

Analyte	SiO <sub>2</sub> (wt.%)	Al <sub>2</sub> O <sub>3</sub> (wt.%)	Fe <sub>2</sub> O <sub>3</sub> (wt.%)	TiO <sub>2</sub> (wt.%)	MgO (wt.%)	CaO (wt.%)	K <sub>2</sub> O (wt.%)	Na <sub>2</sub> O (wt.%)	BaO (wt.%)	MnO (wt.%)	P <sub>2</sub> O <sub>5</sub> (wt.%)	LOI
Ifon Kaolin	41.53	38.2	0.36	0.53	0.094	0.01	0.47	0.31	-	-	-	18.5
Leached kaolin@ 15%	45.6	39.21	0.192	0.2	0.01	<0.001	0.24	0.16	-	<0.001	-	14.39
Zeolite-X 7% 700°C	69.31	13.51	2.03	0.14	1.64	3.11	3.29	1.73	-	-	0.02	5.22
Zeolite-X 15% 700°C	68.93	12.05	0.32	0.17	2	4.1	3.4	1.56	0.01	0.28	0.04	7.14
Zeolite-X 7% 900°C	68.22	12.97	2.26	0.07	1.41	2.65	3.14	1.67	-	-	0.01	7.6
Zeolite-X 15% 900°C	66.17	10.69	0.32	0.14	1.98	3.83	3.32	1.48	0.01	0.19	0.01	11.86

IZX 7%\_700°C represents zeolite-X from Ifon leached with 7% diluted acids and calcined at 700°C

IZX 7%\_900°C represents zeolite-X from Ifon leached with 7% diluted acids and calcined at 900°C

IZX 15%\_700°C represents zeolite-X from Ifon leached with 15% diluted acids and calcined at 700°C

IZX 15%\_900°C represents zeolite-X from Ifon leached with 15% diluted acids and calcined at 900°C

constituents are Fe<sub>2</sub>O<sub>3</sub>, TiO<sub>2</sub>, MgO, CaO, K<sub>2</sub>O, Na<sub>2</sub>O, etc. The chemical composition of the leached kaolin (7 and 15%) is similar, and so only the result obtained with 15% is presented here. After the leaching process, the compounds' composition changes were observed. The amount of SiO<sub>2</sub> increased from 41.5 to 45.6 wt.% while the Al<sub>2</sub>O<sub>3</sub> content slightly increased from 38.2 to 39.21 wt.%. The amounts of the impurity compounds were slightly lowered after the leaching process, ultimately leading to increased alumina and silica contents. The content of Fe<sub>2</sub>O<sub>3</sub> decreased from 0.36 to 0.192 wt.%, and TiO<sub>2</sub> from 0.53 to 0.2 wt.%, K<sub>2</sub>O from 0.47 to 0.24 wt.% and Na<sub>2</sub>O from 0.31 to 0.16 wt.%. Other impurity compounds were found to be in trace quantities. On processing the sample from leached kaolin state to zeolite-X, the amount of Al<sub>2</sub>O<sub>3</sub> on average decreased by about 68%, while SiO<sub>2</sub>, on the other hand, increased by an average of 49% for all zeolite samples. The amount of some hitherto minor constituents increased after the zeolite conversion. This means there were reactions between the Al and the chemicals used in converting the metakaolin to zeolite.

Fe<sub>2</sub>O<sub>3</sub>, MgO, CaO, K<sub>2</sub>O, and Na<sub>2</sub>O increased significantly after zeolite-X synthesis. Only the Fe<sub>2</sub>O<sub>3</sub> content of the samples leached with 7% of the diluted acids increased. An explanation for the increment could be due to the incomplete dissolution of the iron oxide at this acid concentration. A comparison of the calcination temperature effects shows that at 900°C, the amounts of Al<sub>2</sub>O<sub>3</sub> and SiO<sub>2</sub> were slightly decreased relative to that at 700°C. This could be due to the increased loss on ignition (LOI) observed for these samples. Also, the higher the amount of acid used, the lower the yield of SiO<sub>2</sub> and Al<sub>2</sub>O<sub>3</sub>. The values of SiO<sub>2</sub>/Al<sub>2</sub>O<sub>3</sub> for the zeolite-X samples range from 5.13 to 6.19, implying that the zeolite-X samples with 7% acid dilution, fall within the range of values for zeolite-X as reported by Mendoza (2017). The samples leached with 15% diluted acid had SiO<sub>2</sub>/Al<sub>2</sub>O<sub>3</sub> values slightly higher than 5.6.

### 3.2 Fourier transform infra-red (FTIR)

The FTIR spectra of the zeolite samples leached with 7 and 15% acid dilution and calcined at 700°C and 900°C are shown in Fig. 1. The obtained spectra are similar to those of a typical zeolite-

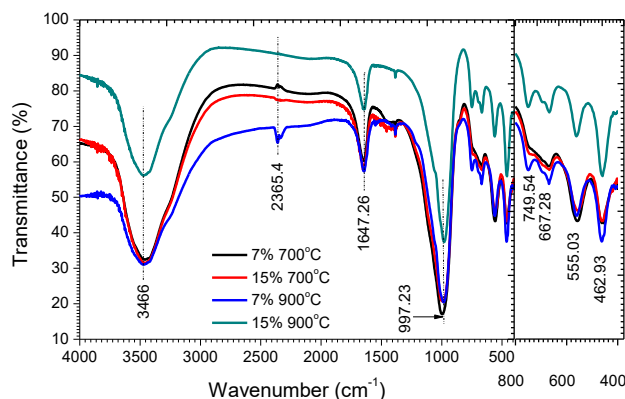


Fig. 1 Fourier Transform Infra-red (FTIR) spectra of zeolite-X samples leached with 7 and 15% diluted acids and calcined at 700 and 900°C. The insert on the right expands the wavenumber from 400  $\text{cm}^{-1}$  to 800  $\text{cm}^{-1}$  for more clarity.

X crystal in the literature, although with slight variations in the wavenumbers (Otieno *et al.* 2021, Srilai *et al.* 2019). The wavenumbers at 749  $\text{cm}^{-1}$ , 667  $\text{cm}^{-1}$ , and 555  $\text{cm}^{-1}$  were slightly lower, while those at 997  $\text{cm}^{-1}$  and 462  $\text{cm}^{-1}$  were slightly higher. The differences with the standard could be attributed to the differences in  $\text{Al}_2\text{O}_3$  content. The characteristic wavenumbers were observed at 3466  $\text{cm}^{-1}$ , 1647  $\text{cm}^{-1}$ , 997  $\text{cm}^{-1}$ , 749  $\text{cm}^{-1}$ , 667  $\text{cm}^{-1}$ , 555  $\text{cm}^{-1}$  and 462  $\text{cm}^{-1}$  respectively.

The band at 1647  $\text{cm}^{-1}$  is attributed to the deformation of  $\text{H}_2\text{O}$  due to incomplete dehydration of the zeolite, while the band at 3466  $\text{cm}^{-1}$  is due to the OH-stretching of water molecules inside the zeolite (Ifitahiyah *et al.* 2018). The intense peak at 997  $\text{cm}^{-1}$  is due to asymmetric stretching of the Si-O-T band, where T represents either Si or Al (Ma *et al.* 2021). The vibration, length, and angle of the Si-O-T bond with different distributions of Si and Al atoms in the framework affect the framework's structure and chemical environment. Based on this peak alone, the obtained zeolite resembles zeolite-Y more than zeolite-X (Wang *et al.* 2013). The peak observed at 749  $\text{cm}^{-1}$  is also attributed to the asymmetric stretching of the bonds, while the peak at 667  $\text{cm}^{-1}$  is due to the symmetric stretching of the bonds. The band at 555  $\text{cm}^{-1}$  is attributed to a double ring formation, while the band at 462  $\text{cm}^{-1}$  is from T-O bending (Zhu *et al.* 2019). The zeolite bands from samples calcined at 900°C differ slightly from those at 700°C, especially between wavenumbers at 600-800  $\text{cm}^{-1}$ . The peaks for samples at 900°C calcination temperature are more developed than those at 700°C.

### 3.3 X-ray diffraction (XRD)

The X-ray powder diffraction patterns for the zeolite-X samples are shown in Fig. 2. The obtained patterns closely resemble that of the typical Faujasite NaX zeolite in the literature (D. Chen *et al.* 2012). There are slight changes in the samples' peak intensities and Bragg angles. Calcinating the kaolin sample at 700°C and 900°C affected the zeolite-X samples' diffraction patterns. Some of the characteristic peaks in the sample calcined at 700°C were missing compared to those at 900°C. This implies that the degree of zeolite formation in samples calcined at 900°C was slightly better than those calcined at 700°C. In addition to the diffraction peaks observed in the zeolite-X crystals,

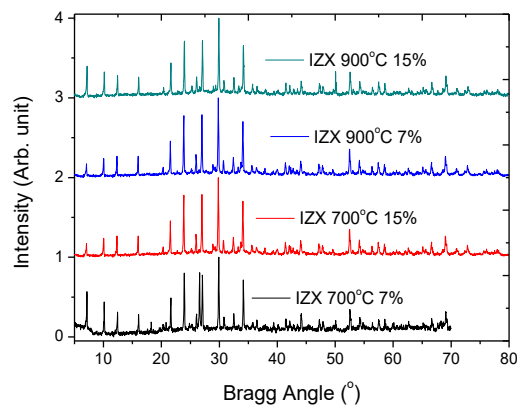


Fig. 2 X-ray powder diffraction patterns of zeolite-X samples measured at room temperature

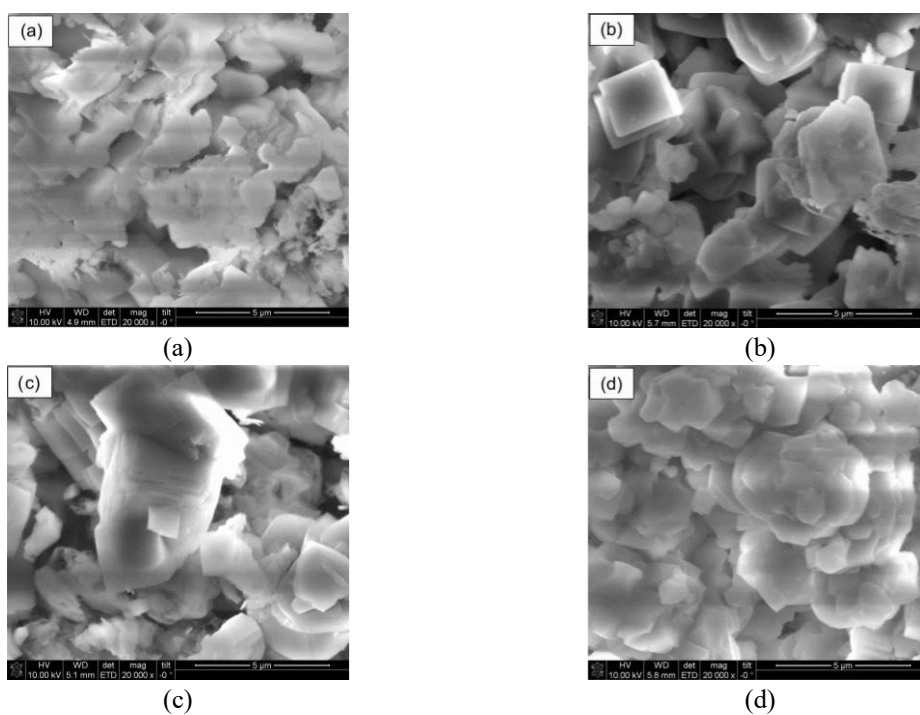


Fig. 3 Scanning Electron Microscope images of the zeolite-X crystals showing (a) Sample leached with 7% of diluted acids and calcined at 700°C, (b) Sample leached with 15% of diluted acids and calcined at 700°C, (c) Leached with 15% of diluted acids and calcined at 900°C and (d) Leached with 15% of diluted acids and calcined at 900°C

other phases were also present in the sample, although in small quantities. Based on the report by Georgiev *et al.* (2013) for kaolin transformed to zeolite NaX, a small amount of quartz ( $\text{SiO}_2$ ) and Andalusite ( $\text{Al}_2(\text{SiO}_4)\text{O}$ ) were observed in addition to the main constituent phase. It is also believed that some of the observed peaks are related to the zeolite P crystals.

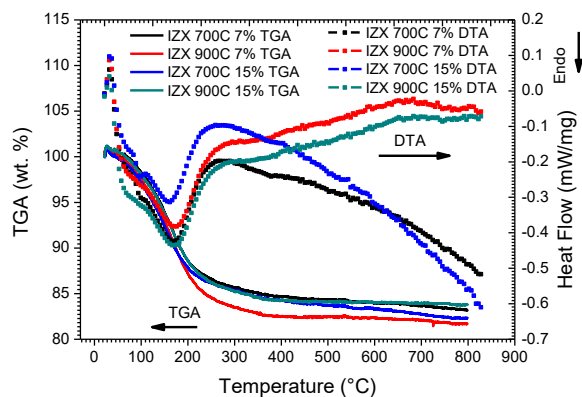


Fig. 4 Thermogravimetric - Differential Thermal Analysis (TG/DTA) plots of the zeolite-X samples measured on heating from 20°C to 800°C

### 3.4 Scanning electron microscopy (SEM)

The Scanning electron microscope images showing the morphology of the zeolite-X samples are shown in Fig. 3. The zeolite leached with 7% acid dilution and calcined at 700°C (Fig. 3(a)) indicates the presence of many tiny grains and a few large grains. The particle sizes range from 1 to 5  $\mu\text{m}$ , and most grains are quasi-cubic in morphology. For the zeolite leached with 15% acid dilution and calcined at 700°C (Fig. 3(b)), there appears to be a gradual change in the shape of the grains. The grains are seen to be agglomerating, and the quasi-cubic grain morphology gradually changes to irregularly shaped grains. The average particle sizes of the grains become larger than that of the former zeolite sample.

The micrograph for the zeolite leached with 7% acid dilution and calcined at 900°C (Fig. 3(c)) shows that some grains look quasi-cubic while others look amorphous. For the zeolite leached with 15% acid dilution and calcined at 900°C (Fig. 3(d)), the particle size of the grains is smaller compared to the sample in Fig. 3(c). There is also no clearly-defined shape for the grains, although some appear to be quasi-spherical. As the kaolin sample calcination temperature increases, the zeolite-X crystals' average grain size increases. The grains are also uniform except where some agglomeration took place. Previous reports in the literature suggest that in the synthesis of zeolite-X, especially when the  $\text{SiO}_2/\text{Al}_2\text{O}_3$  ratio is high, traces of zeolite P are usually observed, corroborating the observation with the X-ray diffraction (Muskoya *et al.* 2015).

### 3.5 Thermal analysis (TG/DTA)

The thermal analysis of the zeolite-X samples using TG/DTA is shown in Fig. 4. The TG of the zeolite samples shows that as the temperature increases from 20°C to 200°C, there was a steep decline in the weight of the samples leading to the loss of about 13 wt.%.

The reduction in mass is due to moisture loss from both the surface of the zeolite crystals and from inside the channels. With a further temperature increase, the weight loss rate decreases gradually to 800°C. At this final temperature, losses in weight ranging from 16.3% to 18.3% for the zeolite 15%\_900°C sample and 7%\_900°C sample, respectively, were obtained. The zeolite samples

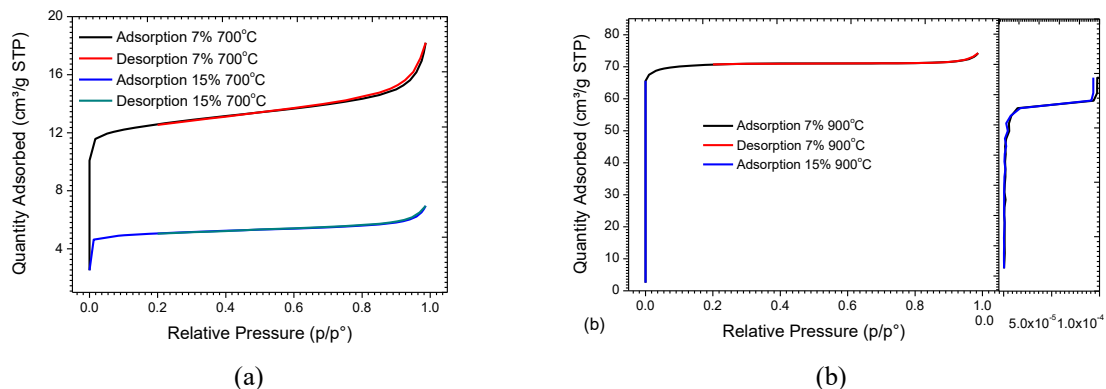


Fig. 5 Plots of the adsorption-desorption isotherms for (a) The zeolite-X samples leached with different concentrations of acid, calcined at 700°C and (b) The zeolite-X samples leached with different concentrations of acid, calcined at 900°C. The graph on the right enlarges the diagram showing the relative pressure in the range of  $5 \times 10^{-5}$  to  $1 \times 10^{-4}$

are structurally stable from 200°C to 800°C after the initial loss in weight attributed to the loss of moisture from hydration complexes formed with exchangeable cations. This is an important property for zeolites used in catalysis and as adsorbents (Georgiev *et al.* 2013). No significant weight reduction was observed for the metakaolin samples since the physically and chemically adsorbed water was washed and removed by heat treatment.

The DTA of the samples showed that as the temperature increased, a negative heat flow was obtained up to 162°C where an endothermic reaction occurred. A similar trend was observed in the zeolite samples, with slight variation in the heat flow values from -0.3124 to -0.4318 mW/mg. Further increment in temperature led to a positive heat flow while a broad exothermic peak was observed at 300°C. Above this temperature, the zeolites from kaolin samples calcined at 900°C showed markedly different characteristics than those at 700°C. The samples calcined at 900°C maintained a positive heat flow, but those calcined at 700°C had a negative heat flow. This difference in sample behaviour at higher temperatures could be due to the degree of zeolite formed in both categories of zeolites.

### 3.6 Braunauer-Emmett-Teller (BET)

The adsorption-desorption isotherms for the zeolite-X samples are shown in Fig. 5. Gas adsorption is the gas sticking on the zeolite-X particles on all possible surfaces, including those inside the pores. As the gas pressure over the zeolite particle increases, the adsorption increases at a particular temperature. In the same way, removing nitrogen from the surface of the zeolite and all possible surfaces inside the pores is known as desorption. As the pressure of the gas decreases, the desorption rate increases. The first edge of the adsorption shows the region of complete monolayer coverage, indicating the zeolite's non-porous nature. The sample calcined at a temperature of 900°C exhibited the type II isotherm associated with unrestricted monolayer-multilayer adsorption. This isotherm is usually found when adsorption occurs on nonporous powders or powders whose diameters exceed those of micro-pores, and the inflection point occurs near the completion of the first adsorbed monolayer. As the concentration of the acid used in leaching increased, the gas

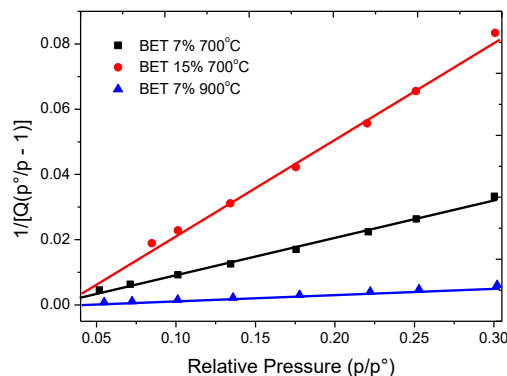


Fig. 6 The plot of the zeolite-X samples showing BET as a function of relative pressure

Table 2 A table showing the parameters from the Nitrogen adsorption isotherm

Parameters Measured	IZX 7%_700°C	IZX 7%_900°C	IZX 15%_700°C	IZX 15%_900°C
Single point surface Area (m <sup>2</sup> /g)	39.2365	215.492	15.7006	-
BET Surface Area (m <sup>2</sup> /g)	38.8617	212.5036	15.1536	-
Langmuir Surface Area (m <sup>2</sup> /g)	53.4857	305.0091	21.6659	274.1116
Single point total Pore	0.028147	0.114878	0.010768	-
Volume (cm <sup>3</sup> /g)	28.9713	21.6238	28.423	-
Avg. Pore width (Å)	28.9713	21.6238	28.423	-

adsorption and desorption rate of the gas became higher. This suggests that samples calcined at this temperature are non-porous with narrower pore sizes and smaller particle diameters.

The samples calcined at a temperature of 900°C exhibit the type I isotherm, characteristic of microporous solids such that the exposed surface is inside the micro-pores with the minimal external surface for further adsorption and also concave to the P/P<sup>0</sup> axis as the plot approaches 1. The sample leached with 15% of the diluted acids and calcined at 900°C could not reach full isotherm as the measurement terminated when the p/p<sup>0</sup> was only  $1 \times 10^{-4}$ . The samples calcined at 900°C adsorbed more nitrogen than those calcined at 700°C.

The BET plot of the zeolite X samples is shown in Fig. 6, while the parameters obtained from the adsorption isotherms are shown in Table 2. The graphs were obtained using the classical BET expression against the relative pressure. The gas adsorption in the 15%\_700°C sample was the highest, with a value of 0.08 at a relative pressure of 0.3. It is followed by the sample with 7%\_700°C with a value of 0.03 and 7%\_900°C with a value of almost 0. The BET values for the 7%\_900°C sample could not be obtained because the adsorption-desorption isotherm could not be obtained.

The mean particle diameter of the zeolite-X from the BET measurement is obtained using Eq. (1).

$$BET = \frac{6000}{\text{surface area}} * \text{density of powder} \quad (1)$$

It was assumed that the particles are non-porous, monodispersed, and spherical in shape and that

the density of the material corresponds to its theoretical density. The BET surface area for the 7%-700°C zeolite sample is 38.8617 m<sup>2</sup>/g and 15.153 m<sup>2</sup>/g for the 15%\_700°C zeolite sample. The BET value for the 7%\_900°C zeolite sample is 212.50 m<sup>2</sup>/g, while that for the 15%\_900°C zeolite sample could not be obtained because the measurement terminated very early. This means the surface areas of samples calcined at 900°C are about 7 orders higher than those at 700°C. The result is also similar to the Langmuir surface area result, where the volume of the pores generated in samples calcined at 900°C was higher than at 700°C. However, the pore widths for samples calcined at 900°C were smaller (21.62 Å) than those at 700°C (28 Å). The average particle size of the samples calcined at 900°C is about 6 orders of magnitude (282 Å) lower than that calcined at 700°C (1544 Å).

#### 4. Conclusions

The impact of calcination temperature and leaching on kaolin deposits from Ifon, Nigeria, was thoroughly studied.

- Upon analyzing the kaolin and zeolite-X crystals, it was observed that zeolite formation led to an increase in silica content and minor elements.
- It was determined from the thermal studies, BET isotherm, X-ray diffraction, and microscopic analysis that the zeolites calcined at 900°C demonstrated superior properties compared to those at 700°C.
- However, applying different leaching concentrations did not significantly affect the properties of the zeolite-X samples obtained.

#### Acknowledgments

The authors thank Dr. Mauricio Schieda at the Helmholtz Zentrum Hereon for access and support with the BET measurements.

The authors have no relevant financial or non-financial interests to disclose for the paper.

#### References

- Abdullahi, T., Harun, Z. and Othman, M.H.D. (2017), "A review on sustainable synthesis of zeolite from kaolinite resources via hydrothermal process", *Adv. Powd. Technol.*, **28**, 1827-1840. <http://doi.org/10.1016/j.appt.2017.04.028>.
- Adeoye, J.B., Omoleye, J.A., Ojewumi, M.E. and Babalola, R. (2017), "Synthesis of zeolite Y from kaolin Using novel method of dealumination", *Int. J. Appl. Eng. Res.*, **12**(5), 755-760.
- Alaba, P.A., Sani, Y.M. and Daud, W.M.A.W. (2015), "Synthesis and characterization of hierarchical nanoporous HY zeolites from acid-activated kaolin", *Chin. J. Catalys.*, **36**, 1846-1851. [https://doi.org/10.1016/S1872-2067\(15\)60962-7](https://doi.org/10.1016/S1872-2067(15)60962-7).
- Alaba, P.A., Sani, Y.M., Mohammed, I.Y., Abakr, Y.A. and Daud, W.M.A.W. (2017), "Synthesis of hierarchical nanoporous HY zeolites from activated kaolin, a central composite design optimization study", *Adv. Powd. Technol.*, **28**, 1399-1410. <https://doi.org/10.1016/j.appt.2017.03.008>.
- Andrade, F.R.D.D., Yogi, M.T.A.G., Gomes, E.B. and Shinzato, M.C. (2020), "Extent of zeolite synthesis via alkaline fusion from tailings dam sediments", *Environ. Earth Sci.*, **79**, 371-379. <https://doi.org/10.1007/s12665-020-09118-9>.

- Atta, A.Y., Ajayi, O.A. and Adefila, S.S. (2007), "Synthesis of faujasite zeolites from kankara kaolin clay", *J. Appl. Sci. Res.*, **3**(10), 1017-1021.
- Chen, D., Hu, X., Shi, L., Cui, Q., Wang, H. and Yao, H. (2012), "Synthesis and characterization of zeolite X from lithium slag", *Appl. Clay Sci.*, **59-60**, 148-151. <https://doi.org/10.1016/j.clay.2012.02.017>.
- Chen, J. and Lu, X. (2018), "Synthesis and characterization of zeolites NaA and NaX from coal gangue", *J. Mater. Cycles Waste Manag.*, **20**, 489-495. <https://doi.org/10.1007/s10163-017-0605-5>.
- Chouafa, M., Idres, A., Bouhedja, A. and Talhi, K. (2015), "Chemical treatment of kaolin. Case study of kaolin from the Tamazert-Jijel Mine", *Min. Sci.*, **22**, 171-180. <https://doi.org/10.5277/msc152214>.
- Georgiev, D., Bogdanov, B., Markovska, I. and Hristov, Y. (2013), "A study of the synthesis and structure of zeolite NaX", *J. Chem. Technol. Metall.*, **48**(2), 168-173.
- Hartanto, D., Iqbal, R.M., Shahbihi, W.E., Santoso, E., Fabsuri, H. and Iryani, A. (2017), "Effect of H<sub>2</sub>O/SiO<sub>2</sub> molar ratio on direct synthesis of ZSM-5 from Bangkok's kaolin without pretreatment", *Malay. J. Fund. Appl. Sci.*, **13**(4), 817-820. <https://doi.org/10.11113/mjfas.v13n4.916>.
- Iftitahiyah, V.N., Prasetyoko, D., Nur, H. and Bahruji, H. (2018), "Synthesis and characterization of zeolite NaX from Bangka Belitung Kaolin as alternative precursor", *Malay. J. Fund. Appl. Sci.*, **14**(4), 414-418. <https://doi.org/10.11113/mjfas.v14n4.964>.
- Khaleque, A., Alam, M.M., Hoque, M., Mondal, S., Haider, J.B., Xu, B., Johir, M.A.H., Karmakar, A.K., Zhou, J.L., Ahmed, M.B. and Moni, M.A. (2020), "Zeolite synthesis from low-cost materials and environmental applications: A review", *Environ. Adv.*, **2**, 100019. <https://doi.org/10.1016/j.envadv.2020.100019>.
- Khalifah, S.N., Aini, Z.N., Hayati, E.K., Aini, N. and Prasetyo, A. (2018), "Synthesis and characterization of mesoporous NaY zeolite from natural Blitar's kaolin", *International Conference on Advanced Materials for Better Future Surakarta, Indonesia 2017*, Surakarta, Indonesia, September.
- Kirdeciler, S.K. and Akata, B. (2020), "One pot fusion route for the synthesis of zeolite 4A using kaolin", *Adv. Powd. Technol.*, **31**, 4336-4343. <https://doi.org/10.1016/j.appt.2020.09.012>.
- Król, M. (2020), "Natural vs. synthetic zeolites", *Crystals*, **10**, 621-628. <https://doi.org/10.3390/cryst10070622>.
- Li, J., Corma, A. and Yu, J. (2013), "Synthesis of new zeolite structures", *Chem. Soc. Rev.*, **44**, 7112-7127. <https://doi.org/10.1039/C5CS00023H>.
- Ma, Y.K., Rigolet, S., Michelin, L., Paillaud, J.L., Mintova, S., Khoerunnisa, F., Daou T.J. and Ng, EP (2021), "Facile and fast determination of Si/Al ratio of zeolites using FTIR spectroscopy technique", *Micropor. Mesopor. Mater.*, **311**, 110683. <https://doi.org/10.1016/j.micromeso.2020.110683>.
- Mendoza, J.G.G. (2017), "Synthesis and applications of low silica zeolites from Bolivian clay and diatomaceous earth", Ph.D. Dissertation, Lulea University of Technology, Lulea, Sweden.
- Mgbemere, H.E., Lawal, G.I., Ekpe, I.C. and Chaudhary, A.L. (2018), "Synthesis of zeolite-A using kaolin samples from Darazo, Bauchi State and Ajebo, Ogun State in Nigeria", *Niger. J. Technol.*, **37**(1), 87-95. <https://doi.org/10.4314/njt.v37i1.12>.
- Muskoya, N.M., Petrik, L.F., Hums, E., Kuhnt, A. and Schwieger, W. (2015), "Thermal stability studies of zeolites A and X synthesized from South African coal fly ash", *Res. Chem. Intermed.*, **41**, 575-582. <https://doi.org/10.1007/s11164-013-1211-3>.
- Ojumu, T.V., Plessis, P.W.D. and Petrik, L.F. (2016), "Synthesis of zeolite A from coal fly ash using ultrasonic treatment - A replacement for fusion step", *Ultrason. Sonochem.*, **31**, 342-349. <https://doi.org/10.1016/j.ultsonch.2016.01.016>.
- Otieno, S., Kowenje, C., Kengara, F. and Mokaya, R. (2021), "Effect of kaolin pre-treatment method and NaOH levels on the structure and properties of kaolin-derived faujasite zeolites", *Mater. Adv.*, **2**, 5997-6010. <https://doi.org/10.1039/D1MA00449B>.
- Pavlov, M.L., Travkina, O.S., Khazipova, A.N., Basimova, R.A., Shavaleeva, N.N. and Kutepov, B.I. (2015), "Synthesis of Ultrafine and binder-free granular zeolite Y from kaoli", *Petrol. Chem.*, **55**(7), 552-556. <https://doi.org/10.1134/S0965544115070105>.
- Salahudeen, N. and Ahmed, A.S. (2017), "Synthesis of hexagonal zeolite Y from Kankara kaolin using a split technique", *J. Inclus. Phenom. Macrocycl. Chem.*, **87**, 14-156. <https://doi.org/10.1007/s10847-016-0686-0>.

- Srilai, S., Tanwongwan, W., Onpetch, K., Wongkitikun, T., Panpiemrasda, K., Panomsuwan, G. and Eiad-Ua, A. (2019), "Synthesis of zeolite X from bentonite via hydrothermal method", *Mater. Sci. Forum*, **990**, 144-148. <https://doi.org/10.4028/www.scientific.net/MSF.990.144>.
- Verboekend, D., Nuttens, N., Locus, R., Aelst, J.V., Verolme, P., Groen, J.C., Pe´rez-Rami´rez, J. and Sels, B.F. (2016), "Synthesis, characterisation, and catalytic evaluation of hierarchical faujasite zeolites: milestones, challenges, and future directions", *Chem. Soc. Rev.*, **45**, 3331-3352. <https://doi.org/10.1039/C5CS00520E>.
- Wang, C., Zhou, J., Wang, Y., Yang, M., Li, Y. and Meng, C. (2013), "Synthesis of zeolite X from low-grade bauxite", *J. Chem. Technol. Biotechnol.*, **88**(7), 1350-1357. <https://doi.org/10.1002/jctb.3983>.
- Zhu, T., Zhang, X., Han, Y., Liu, T., Wang, B. and Zhang, Z. (2019), "Preparation of zeolite X by the Aluminum residue from coal fly ash for the adsorption of volatile organic compounds", *Front. Chem.*, **7**, 341-348. <https://doi.org/10.3389/fchem.2019.00341>.

CC